Numerical Solution of Three-Dimensional Navier-Stokes Equations Showing Trailing Tip Vortices

J. F. THOMPSON* AND S. P. SHANKS†
Mississippi State University, Miss.

AND

J. C. WU‡
Georgia Institute of Technology, Atlanta, Ga.

Numerical solution of the incompressible Navier-Stokes equations in integro-differential form is applied to time-dependent flow about a rectangular slab at an angle of attack. With this formulation the solution is obtained in the entire unbounded flowfield, but with actual computation required only in regions of significant vorticity. This allows considerable reduction in computer storage, since only points in regions of significant vorticity need be stored at any particular time. The computational field thus expands in time. (This method is not to be confused with "vortex methods" using discrete vortices and images.) The finite numerical calculation field in the integro-differential formulation is, in effect, infinite, and the necessity of locating "infinity" at a finite distance is avoided. Although it is not necessary in this numerical method to calculate the velocity at points outside the region of nonzero vorticity, the velocity at these points and, in fact, to infinity, is determined by the solution via an integral over the vorticity distribution. The method requires two orders of magnitude less computer storage than do methods based on the differential formulation. Results have been obtained for the development of trailing tip vortices and the force coefficients.

Introduction

DUE to the nonlinearity of the differential equations governing incompressible viscous fluid motion, i.e., the Navier-Stokes equations, exact solutions have been obtained in only a few very specialized cases. Furthermore, a general analytic solution of this fourth-order, nonlinear system of partial differential equations is not a foreseeable possibility. Attention, therefore, has been directed over the past seventy years to approximate methods, primarily of the boundary-layer type in which the Navier-Stokes equations are replaced by a lower order differential system, neglecting certain derivatives tangential to solid surfaces in comparison with normal derivatives. However, the boundary-layer equations, being of lower order than the Navier-Stokes equations, simply do not contain some of the essential information concerning some fluid flows, in particular those involving separation. There has, therefore, been a rapidly increasing effort in the past decade directed toward numerical solution of the full Navier-Stokes equations. Unfortunately, the key to the success of the boundary-layer approximation has been the greatest obstacle to numerical solution of the full equations.

The boundary-layer concept is a manifestation of a basic property of the Navier-Stokes equations—the tendency for large velocity gradients to be confined to relatively small regions of the field for large Reynolds number—and the success of boundary-layer theory in describing a wide range of fluid flow is evidence of the prevalence of this property. This means that the mesh points of a finite-difference computation field must be very closely spaced in certain relatively small regions of the flowfield where the gradients are large, e.g., in the vicinity of solid surfaces, while there is no need for such a fine mesh in most of the field. This is especially true if the forces on solid bodies are to be calculated, since the surface pressure distribution is dependent on the normal (to the surface) derivative of the vorticity. It is possible for a numerical solution to yield an accurate representation of large scale phenomena, such as shed vortices, etc., and still be incapable of predicting lift and drag accurately unless the mesh is very closely spaced in the vicinity of the solid surfaces. The accurate prediction of the forces on solid bodies depends directly on the accurate representation of the large gradients near the solid surfaces.

The problems with numerical solution become more acute at higher Reynolds numbers, since the gradients increase in magnitude as the Reynolds number increases. For this reason the mesh size in the vicinity of solid surfaces must be reduced as the Reynolds number is increased if accuracy in surface pressure and force calculations is to be maintained. However, while the gradients become stronger, they are confined to a smaller region at higher Reynolds numbers. Thus, as the Reynolds number increases, a smaller mesh is required near solid surfaces, but the lateral extent of the region in which a coarse mesh would suffice increases.

The incompressible Navier-Stokes equations, however, are elliptic in space, so that the boundary conditions must be specified on the entire boundary, and the solution must be obtained simultaneously on the entire field. It is not possible to isolate any portion of the field and obtain the solution in only that portion. Therefore, with the differential equations approximated by difference equations, the entire flowfield must be covered by a mesh. It is possible, however, to circumvent the need for such large fields by reformulating the incompressible Navier-Stokes system as an integro-differential system.[1-3] Numerical solutions based on the integro-differential formulation, rather than the more conventional differential formulation of the Navier-Stokes equations, are benefited, rather than hindered, by the tendency of large gradients to concentrate in relatively small regions. With this formulation actual numerical computation is required only in the regions of significant vorticity,

Presented at the AIAA Computational Fluid Dynamics Conference, Palm Springs, Calif., July 19–20, 1973; submitted July 30, 1973; revision received December 18, 1973. Research sponsored by U.S. Army Research Office—Durham.

Index categories: Viscous Nonboundary-Layer Flows; Nonsteady Aerodynamics; Jets, Wakes, and Viscid-Inviscid Flow Interactions.

* Associate Professor. Member AIAA.

† Graduate Research Assistant. Student Member AIAA.

‡ Professor. Associate Fellow AIAA.

yet the solution is still obtained in the entire field as required by the elliptic nature of the Navier-Stokes equations. As shown in the next section, it is thus necessary to store only those points of the field at which the vorticity is significant at any given time. The computational field thus expands in time.

This formulation does not, in itself, introduce any approximation. It should not be confused with so-called "vortex methods," in which the flow is represented by discrete vortices and their images distributed throughout the field. Thus, the numerical formulation of Payne, used for the two-dimensional circular cylinder[4] and the plane jet[5] (also by Ingham[6] for the circular cylinder), bears some surface resemblance to the present formulation, but is fundamentally different, being based on the use of discrete line vortices and their images in any solid surfaces present, rather than on the integro-differential formulation of the governing equation. It is thus necessary in this formulation that the image points in any curved solid surfaces be located, a requirement that is difficult to fulfill for general surfaces. The recent formulation of Chorin,[7] using "vortex blobs" and statistical simulation of vorticity generation and dispersal, is formally equivalent in the limit of a continuous vorticity distribution to the integro-differential formulation. In its computational form, however, this formulation relies on statistical averages and thus does not provide pointwise description in either space or time.

The present formulation results in a reduction by two orders of magnitude in the number of computation points, and hence in the computer storage required, and thus makes three-dimensional solutions at least possible for flowfields of meaningful size. The present paper extends the method to the flow about a finite three-dimensional body; the general formulation, verification, and application to the two-dimensional flow about a circular cylinder have been treated elsewhere.[3]

Integro-Differential Formulation

Mathematical Formulation

Incompressible fluid motion is governed by the Navier-Stokes equations with constant density and fluid properties, together with the continuity equation. The pressure may be eliminated as a dependent variable by taking the curl of the Navier-Stokes equations and introducing the vorticity as a dependent variable. The system of differential equations governing the motion is then (with ω, $\mathbf{v}$, and ν the vorticity, velocity, and kinematic viscosity, respectively)

$$\partial\omega/\partial t = \nabla \times (\mathbf{v} \times \omega) + \nu\nabla^2\omega \tag{1}$$

$$\nabla \times \mathbf{v} = \omega \tag{2}$$

$$\nabla \cdot \mathbf{v} = 0 \tag{3}$$

The last two equations together imply the equation

$$\nabla^2\mathbf{v} = -\nabla \times \omega \tag{4}$$

Equation (4), being a Poisson equation, can be expressed in integral representation by the use of Green's Theorem, so that the motion may be described by the following integro-differential system[1]:

$$\mathbf{v}(\mathbf{r}) = \mathbf{V}_\infty + \frac{1}{4\pi}\iiint \frac{(\mathbf{r}'-\mathbf{r}) \times \omega(\mathbf{r}')}{|\mathbf{r}'-\mathbf{r}|^3} \tag{5}$$

$$\partial\omega/\partial t = \nabla \times (\mathbf{v} \times \omega) + \nu\nabla^2\omega \tag{6}$$

Here the integration is over $\mathbf{r}'$, with ω being a function thereof, and the volume integral is over the entire flowfield. The boundary conditions at infinity are contained implicitly in the formulation so that no further specification is necessary. In fact, the finite numerical calculation field in the integro-differential formulation is, in effect, infinite, and the necessity of locating "infinity" at a finite distance, as is required in numerical methods based on the differential formulation, is avoided.

For a given vorticity distribution the solution of Eqs. (2) and (3), i.e., the velocity distribution, is uniquely determined by the specification of either the normal or tangential velocity on the body surface. It is, in fact, not possible to obtain a solution for the velocity with both the normal and tangential components specified on the surface with an arbitrary vorticity distribution. However, for any combination of normal and tangential velocity on the body surface there is some particular vorticity distribution for which the solution of Eqs. (2) and (3), with either this normal velocity or this tangential velocity specified on the surface, will yield the other member of the combination on the surface. This solution of Eqs. (2) and (3) is unique and is thus the only solution for this particular vorticity distribution having this particular combination of normal and tangential velocity on the surface.

Now the solution of Eq. (4) is uniquely determined with a given vorticity distribution only if both the normal and tangential velocity components on the surface are specified. This means that for a given vorticity distribution there are infinitely many surface tangential velocity distributions that may be specified in combination with a given surface normal velocity distribution (and vice versa) for which a solution of Eq. (4) will exist. Now only one of these surface tangential velocity distributions is the one produced by the solution of Eqs. (2) and (3) with this same vorticity distribution and surface normal velocity specification. Thus for any given vorticity distribution there are combinations of normal and tangential surface velocity distributions for which a solution of Eq. (4) exists, but no solution of Eqs. (2) and (3) exists. The converse is not true, since by the vector identity $\nabla^2\mathbf{v} = \nabla(\nabla \cdot \mathbf{v}) - \nabla \times (\nabla \times \mathbf{v})$ and the fact that both the normal and tangential surface velocities may be specified in the solution of Eq. (4), any solution of Eqs. (2) and (3) must also be a solution of Eq. (4).

The point then is this: if the solution of Eqs. (2) and (3) exists for a given vorticity distribution and a given combination of normal and tangential surface velocity distributions (only one member of the combination being *specified*, the other coming from the solution), then this solution is unique and is also the unique solution of Eq. (4) for these conditions (with both members of the surface velocity combination specified). Therefore, the velocity may be obtained by solving Eq. (4) instead of Eqs. (2) and (3), *provided* the vorticity distribution is such that a solution of Eqs. (2) and (3) exists for the specified boundary conditions on both the normal and tangential components of the velocity. If this is not the case then no physical solution exists anyway [although a solution of Eq. (4) would exist]. Thus if the vorticity distribution is physically possible, i.e., one for which a solution of Eqs. (2) and (3) exists with the specified surface velocity, then the velocity calculated from Eq. (5) is the correct physical velocity in the field, and it satisfies surface boundary conditions.

The burden in a physical problem then rests on maintaining a vorticity distribution for which the solution of Eqs. (2) and (3) will exist for a certain specified combination of the normal and tangential velocity on the surface. It is the nature of the parabolic (in time) vorticity equation to maintain a vorticity distribution having this property, provided the initial vorticity distribution is such that a solution [Eqs. (2) and (3)] exists and that the vorticity boundary conditions are evaluated in terms of the specified surface velocity. If this were not so, the Navier-Stokes equations would not be capable of describing a physical flow.

In a numerical solution, if the vorticity distribution is physical [one for which the solution of Eqs. (2) and (3) exists with the specified surface velocity] then Eq. (5) must produce the physical velocity (to within the discretization error). Then, with the boundary conditions for the vorticity evaluated in terms of the specified surface velocity, the use of the velocity from Eq. (5) in the finite-difference approximation of the parabolic vorticity equation will produce a vorticity distribution at the next step that is also physically possible (to within the discretization error). If, through the inadequate representation of the vorticity boundary conditions, the vorticity distribution becomes unphysical, then the velocity produced by Eq. (5) becomes unphysical also. However, no solution of Eqs. (2) and (3) satisfying the velocity boundary conditions will even exist, so that the entire solution is meaningless anyway.

This is, in fact, not the only method of solution in which the question of specification of both normal and tangential velocity components on the body arises and boundary condition satisfaction depends on the maintenance of a proper vorticity distribution by the parabolic equation. In two-dimensional numerical solutions using the vorticity and stream function as dependent variables the velocity is calculated from the stream function, which is given in terms of the vorticity by a Poisson equation.[8] The solution of this equation is uniquely determined by the specification of either the stream function or its normal derivative on the boundary, the former of which is equivalent to the specification of the normal velocity component on the boundary, and the latter is equivalent to the specification of the tangential component. Thus, either the normal or the tangential velocity component on the surface may be specified, but not both. The vorticity distribution must be such that the solution, with either the normal or tangential surface velocity component specified, will produce the desired value of the other component.

It is then not necessary, or even possible, to add a potential flow to the field produced by Eq. (5), as might seem to be the case in view of Eqs. (2) and (3). Since the velocities from Eq. (5) satisfy the specified boundary conditions, the velocities of any added potential flow would be required to vanish on all the boundaries. Then by the maximum principle for Laplace's equation, the only potential solution would be the trivial solution of zero velocity throughout the field.[9]

Numerical Formulation

In the numerical solution the flowfield is divided into elementary cubic cells, each of which is centered on a point of a rectangular grid of constant mesh width. For purposes of identification the following definitions are introduced (Fig. 1): vortex cell—a cell centered on a point having nonzero vorticity; border cell—a cell centered on a point having zero vorticity, but being adjacent to a vortex cell; boundary vortex cell—a cell adjacent to a solid surface boundary; aggregate of vortex cells—the group of all the vortex cells in the flowfield at a given time.

The parabolic (in time) differential equation (6) is approximated in all vortex and border cells by a difference equation using second-order central time differences:

$$\left(\frac{\partial\omega}{\partial t}\right)^n_{ijk} = \frac{\omega^{n+1}_{ijk}-\omega^{n-1}_{ijk}}{2\Delta t} + 0(\Delta t^2) \tag{7}$$

in the Dufort-Frankel formulation.[10] (The subscripts refer to the position (x_i, y_j, z_k) and the superscript to the time t_n. The time step is Δt, and the cell width is h.) All space derivatives are approximated by second-order central space differences:

$$\left(\frac{\partial(\mathbf{v}\times\boldsymbol{\omega})}{\partial x}\right)^n_{ijk} = \frac{1}{2h}[(\mathbf{v}\times\boldsymbol{\omega})^n_{i+1,j,k}-(\mathbf{v}\times\boldsymbol{\omega})^n_{i-1,j,k}]+0(h^2) \tag{8}$$

$$\left(\frac{\partial^2\omega}{\partial x^2}\right)^n_{ijk} = \frac{1}{h^2}[\omega^n_{i+1,j,k}-\omega^{n+1}_{ijk}-\omega^{n-1}_{ijk}+\omega^n_{i-1,j,k}]+0(h^2) \tag{9}$$

In the boundary cells the space derivatives normal to the body surface must use a point one-half cell width away toward the surface. For example, for a boundary cell centered at (x_i, y_j, z_k) adjacent to the surface at $[x_i-(h/2), y_j, z_k]$, the space derivatives are approximated by the following second-order difference forms:

$$\left(\frac{\partial(\mathbf{v}\times\boldsymbol{\omega})}{\partial x}\right)^n_{ijk} = \frac{1}{3h}[(\mathbf{v}\times\boldsymbol{\omega})^n_{i+1,j,k}+3(\mathbf{v}\times\boldsymbol{\omega})^n_{ijk}]+0(h^2) \tag{10}$$

$$\left(\frac{\partial^2\omega}{\partial x^2}\right)^n_{ijk} = \frac{1}{5h^2}[-\omega^n_{i+2,j,k}+10\omega^n_{i+1,j,k}-\tfrac{25}{2}(\omega^{n+1}_{ijk}+\omega^{n-1}_{ijk})+16\omega^n_{i-1/2,j,k}]+0(h^2) \tag{11}$$

In Eq. (10) the boundary condition, $\mathbf{v}=0$ on the surface, has been applied, giving $(\mathbf{v}\times\boldsymbol{\omega})_{i-1/2,j,k}=0$.

The volume integral of Eq. (5) is approximated numerically by

$$\mathbf{v}^n_{ijk} = \frac{h^3}{4\pi}\sum_p\sum_q\sum_m \frac{(\mathbf{r}_{pqm}-\mathbf{r}_{ijk})\times\boldsymbol{\omega}^n_{pqm}}{|\mathbf{r}_{pqm}-\mathbf{r}_{ijk}|^3} + \mathbf{V}_\infty \tag{12}$$

$$(pqm)\neq(ijk)$$

Here the summation is taken only over the aggregate of vortex cells, since the integrand of Eq. (5) is zero elsewhere.

Boundary Conditions

The vorticity on the surface is calculated from Eq. (2) applied on the surface, which condition may be expressed as[1]

$$\boldsymbol{\omega} = \mathbf{n}\times(\partial\mathbf{v}/\partial n) \tag{13}$$

where $\mathbf{n}$ is the unit outward normal to the surface. The derivative normal to the surface in this expression is approximated by a second-order, one-sided difference form so that, since the derivative parallel to the wall is zero by the velocity boundary condition

$$\boldsymbol{\omega}^n_{i-1/2,j,k} = \mathbf{n}_{i-1/2,j,k}\times\frac{1}{3h}[-\mathbf{v}^n_{i+1,j,k}+9\mathbf{v}^n_{ijk}]+0(h^2) \tag{14}$$

Initial Condition

The flow is assumed to start impulsively, so that the initial condition is the potential flow solution, $\mathbf{v}(\mathbf{r})=\mathbf{V}_\infty+\nabla\phi(\mathbf{r})$, with the velocity potential, $\phi(\mathbf{r})$, determined by the system

$$\nabla^2\phi = 0 \tag{15a}$$

$$\partial\phi/\partial n = -\mathbf{V}_\infty\cdot\mathbf{n} \quad \text{on the body surface} \tag{15b}$$

$$\nabla\phi\to 0 \quad \text{at infinity} \tag{15c}$$

Here $\mathbf{n}$ is the unit outward normal on the body surface. By the use of Green's Theorem the solution of this differential system can also be given as the solution of the integral equation[11]

$$\phi(\mathbf{r}) = \frac{1}{2\pi}\int_{S_B}\int\frac{\mathbf{V}_\infty\cdot\mathbf{n}(\mathbf{r}')}{|\mathbf{r}'-\mathbf{r}|}dS - \frac{1}{2\pi}\int_{S_B}\int\frac{(\mathbf{r}'-\mathbf{r})\cdot\mathbf{n}(\mathbf{r}')}{|\mathbf{r}'-\mathbf{r}|^3}\phi(\mathbf{r}')dS \tag{16}$$

Here the integration is over $\mathbf{r}'$, and S_B is the set of points comprising the body surface, excluding the point $\mathbf{r}'=\mathbf{r}$. The first integral is, of course, known from the body shape.

For a body that is symmetric about the $z=0$ plane, the integrations in Eq. (16) may be confined to the set, S_0, of points comprising the half-body on the positive side of this plane by writing Eq. (16) as

$$\phi(\mathbf{r}) = \frac{1}{2\pi}\int_{S_0}\int\mathbf{V}_\infty\cdot\left(\frac{\mathbf{n}(\mathbf{r}')}{|\mathbf{r}'-\mathbf{r}|}+\frac{\mathbf{n}(\mathbf{R}')}{|\mathbf{R}'-\mathbf{r}|}\right)dS - \frac{1}{2\pi}\int_{S_0}\int\left(\frac{(\mathbf{r}'-\mathbf{r})\cdot\mathbf{n}(\mathbf{r}')}{|\mathbf{r}'-\mathbf{r}|^3}+\frac{(\mathbf{R}'-\mathbf{r})\cdot\mathbf{n}(\mathbf{R}')}{|\mathbf{R}'-\mathbf{r}|^3}\right)\phi(\mathbf{r}')dS \tag{17}$$

where

$$\mathbf{R}' = \mathbf{r}'-2(\mathbf{r}'\cdot\mathbf{k})\mathbf{k} \tag{18a}$$

$$\mathbf{n}(\mathbf{R}') = \mathbf{n}(\mathbf{r}')-2[\mathbf{k}\cdot\mathbf{n}(\mathbf{r}')]\mathbf{k} \tag{18b}$$

$$\phi(\mathbf{R}') = \phi(\mathbf{r}') \tag{18c}$$

Here the point $\mathbf{r}'=\mathbf{r}$ is excluded from the integration over the first term of each integral.

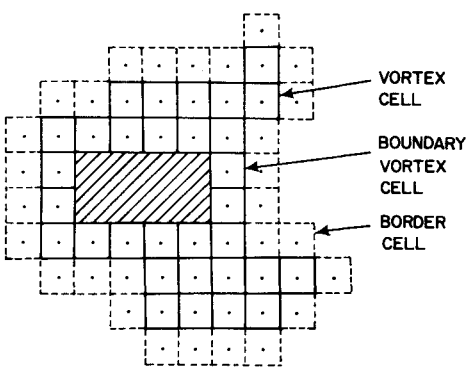

Fig. 1 Cell configuration.

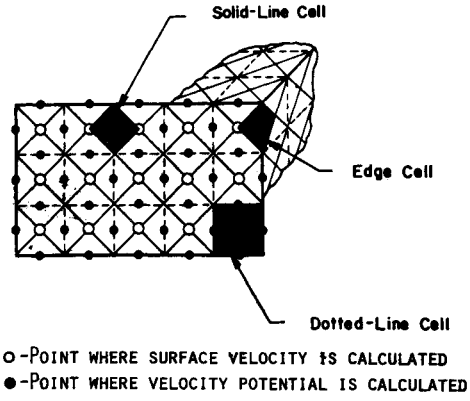

Fig. 2 Surface cell configuration.

The cell configuration for each face of the rectangular slab is shown in Fig. 2. The cells that are used in the potential solution are those formed by the solid lines, and the cells formed by the dotted lines are used in the viscous solution. All of the solid-line cells have the same area, although some are shared by two faces, except the cells along the edges on the plane of symmetry, which have half the area of the others. Taking the distance between the dotted lines as the reference length, the area of all the solid-line cells, except those along the edges of the plane of symmetry, is 0.5. As indicated in Fig. 2, the potential is evaluated at the center of each solid-line cell.

With the integrals in Eq. (17) approximated by finite summations over these cells, the integral equation (17) is approximated by a system of linear algebraic equations, one for each cell. The solution of this algebraic system was obtained[11] by point SOR iteration,[12] the optimum acceleration parameter for which was determined by computer experimentation to be unity. The system was irreducibly diagonally dominant and the convergence was extremely rapid, the maximum norm of the change between iterates decreasing generally by an order of magnitude at each iteration.

Surface Pressure and Force Coefficients

Since the velocity is zero on the surface by the boundary conditions, the convective terms in the Navier-Stokes equations vanish on the surface, and the equations reduce to

$$\nabla p = -\mu \nabla \times \omega \tag{19}$$

The surface pressures are calculated from the line integral of this equation over the surface[11] with the derivatives normal to the surface approximated by the same second-order, one-sided difference form given above for the vorticity boundary conditions. The force coefficients then are calculated from these surface pressures and the shear stress evaluated on the body surface.

Computation Procedure

The explicit numerical solution[1] consists of a two-part procedure at each time step: a) first the new vorticity is calculated at the new time from the finite-difference approximation of the parabolic differential equation (6), and b) then the new velocity is calculated from the integral (5) (as approximated by a finite summation) over the new vorticity distribution. Now only those field points with nonzero vorticity need be considered in the calculation of the velocity from the integral over the vorticity distribution, since the integrand is zero where the vorticity is zero. Furthermore, with the space derivatives in the differential equation for the vorticity expressed by second-order central differences, the vorticity can change at each time step only at, or adjacent to, points that had nonzero vorticity at the previous time step. Therefore, the velocity is required for the actual calculation only at points having nonzero vorticity at any given time. (It should be noted that although it is not necessary in this numerical method to calculate the velocity at points outside the region of nonzero vorticity, the velocity at these points and, in fact, to infinity, is determined by the solution, via the integral over the vorticity distribution, and can be calculated whenever desired.)

This then means that the solution in the entire flowfield can be obtained while actually performing calculations only in the region of nonzero vorticity at each time. Therefore, only the points with significant vorticity at a given time need be stored at that time, rather than all the field points as would be required if the numerical solution were based on the differential formulation.

At each time step new values of the vorticity are calculated for each vortex cell and each border cell from the numerical approximation of Eq. (6). In this equation the vorticity is taken as zero at all points not corresponding to vortex cells, so that no vorticity is ever simply discarded. (The simple discarding of the vorticity calculated for the border cell, in the event of no reclassification, results in vorticity flowing out of the field of computation, so that the viscous effects of the wall are eventually obliterated.)[1]

The current set of vortex cells, including those added at the current time step, is then cataloged§ and a new set of border cells surrounding the aggregate of vortex cells is created. Finally, the velocity components are calculated for each vortex cell from the numerical approximation of Eq. (5), with the summation being taken only over those vortex cells within a prescribed range of the cell in question. This process is repeated at each succeeding time step for the duration of the calculations.

Since some small finite value of vorticity must be specified in the numerical solution as the value below which vorticity is considered to be effectively zero, the present integro-differential formulation incorporates a natural means by which the accuracy, and hence the computer time one is willing to expend, may be restricted for a certain application. Comparisons of the results as this minimum vorticity is decreased are given in Ref. 1 for several applications, and a minimum vorticity of 0.01 (non-dimensionalized with reference to the freestream velocity and the cell width) was found to be sufficient.

A second natural approximation which may be employed, if desired, to gain speed at the expense of accuracy is the neglect of all vorticity more distant than some prescribed range from the point in question in the calculation of the velocity from the vorticity distribution by Eq. (5). This is possible because of the rapid decrease with distance of the geometric coefficients of the vorticity in the integrand of this equation. Again an evaluation of the effect of using this approximation in the velocity calculation is given in Ref. 1, where twice the cylinder diameter was found to be sufficient for accuracy in the case of the two-dimensional circular cylinder.

Computer Time Required

The computer time required increases as time progresses, since the computational field becomes larger at each time step as more vortex cells are added. The computer time is also strongly dependent on the influence range beyond which vorticity is neglected in the velocity calculation, since the velocity calculation accounts for the majority of the computation time required at each time step.

The large computer time required by the evaluation of the velocity from the integral over the vorticity field makes the numerical method based on the integro-differential formulation in its present form noncompetitive with methods based on differential formulation in two-dimensional problems. This arises from the fact that the integral solution of Poisson's equation is equivalent, in finite methods, to multiplication by a known square matrix inverse, the order of which is equal to the number of calculation points in the field. The differential solution of Poisson's equation, however, is equivalent, in finite methods, to solving the matrix equation by iteration rather than by inversion.

§ A special catalog procedure[1] is necessary since identification by grid point subscripts would amount to storing the entire rectangular field.

For matrices of any appreciable size, iterative methods of solution, especially with convergence acceleration, are much more efficient than multiplication by the matrix inverse.[12]

There is another point, however, for the field involved in the integro-differential method, including as it does only the points with nonzero vorticity at any time, is smaller than that necessary for differential methods. (The abovementioned restriction of the summation to points within a certain distance of the point in question reduces the size still further.) The latter must, of course, include at all times the entire field ever to be used at any time. Therefore, the matrix inverse used in the integro-differential method is smaller than the matrix to be solved by iteration in the differential methods. There is, then, a cross-over point, the integro-differential method being faster at the earlier time steps than the differential. The situation is reversed, however, as the computational field of the integro-differential method increases with time and the matrix inverse becomes larger. Though always smaller than the matrix of fixed size that is solved iteratively in the differential methods, the matrix inverse of the integro-differential method eventually requires more time for multiplication than is required for iterative solution of the larger matrix of the differential methods.

In three dimensions, however, the integro-differential method is superior in speed at the present state of the art. The relative field matrix size advantage of the integro-differential method over that of the differential is increased by an order of magnitude in three dimensions, as compared with two dimensions. The point at which multiplication by the smaller matrix inverse requires more calculations than the iterative solution of the larger matrix is thus postponed to much larger times in three-dimensional problems. The result is a significant speed advantage of the integro-differential method in three dimensions at the present time.

In this connection it should be mentioned that the computer times given in Ref. 1 are not representative of the speed of the solution. Due to limitations of the storage (both in core and auxiliary) made available to the research reported in Ref. 1, it was necessary to recalculate the geometric coefficients of the vorticity used in the integration in Eq. (5) at each time step. These coefficients are, of course, constant in time and should be calculated only once and stored for subsequent use. The disk storage available to the present research allowed this procedure to be followed efficiently. Since the number of these geometric coefficients is proportional to the square of the number of points in the field, the savings in time thus achieved is quite significant. The present scheme requires about two minutes per step for about 1500 cells on a UNIVAC 1106.

Evaluation and Previous Applications

The results of the numerical method have been compared[1-3] with experimental data and with the results of other numerical solutions for the drag and pressure coefficients and vortex shedding frequency and length for a two-dimensional circular cylinder, and with the analytical solution for the one-dimensional flow above an impulsively accelerated infinite flat plate. With cartesian coordinates the cell Reynolds number must be unity or less for accurate drag prediction for a circular cylinder. The numerical method with cartesian coordinates was capable of predicting the surface pressure distribution for the cylinder also, but with some irregularity due to the angularity of the boundary, for cell Reynolds numbers of unity or less.

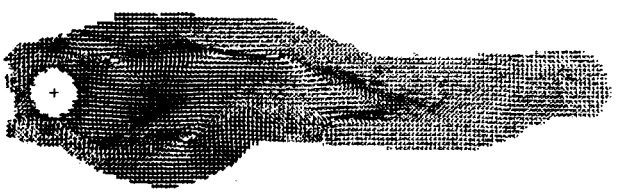

Fig. 3 Vortex street behind circular cylinder – $R = 120$, $T = 18.00$.

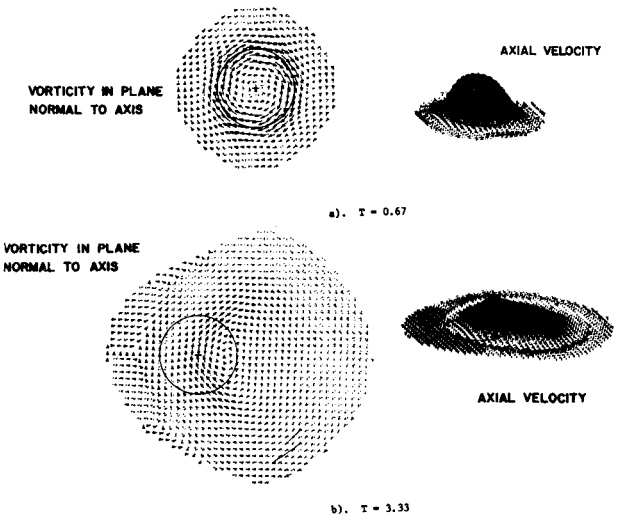

Fig. 4 Circular infinite jet in cross-wind—$R = 30$, velocity ratio = 8.

The numerical method was capable of predicting the time history of the length of the standing vortices behind a two-dimensional solid circular cylinder with accuracy for cell Reynolds numbers of 3 or less, and possibly higher. The method did produce periodic vortex shedding, at a frequency close to the expected value when a vorticity perturbation was introduced, and showed the establishment of a vortex street. The shedding and street formation were surpressed by the addition of a rear splitter plate. Shed vortices behind a two-dimensional circular cylinder are evident in Fig. 3, which also gives a good illustration of the manner in which the computational field is confined to the developing region of significant vorticity. (Time, T, is non-dimensionalized with respect to the cell width and the freestream velocity, R is the cell Reynolds number.)

With the Dufort-Frankel formulation, the maximum time step approaches a finite nonzero lower limit as the Reynolds number approaches infinity, and the solution was run for the two-dimensional circular cylinder at a Reynolds number of 10^6 without instability.[1] As with other numerical methods, however, the accuracy of the calculation of surface pressure and force coefficients with a fixed cell size decreases as the Reynolds number increases, so that more cells and hence more computer time must

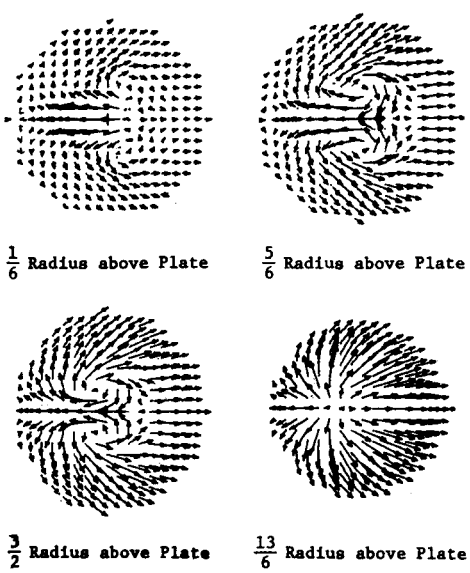

Fig. 5 Jet in cross-wind. Velocity vectors in planes parallel to plate—$R = 12$, velocity ratio = 8, $T = 1.13$.

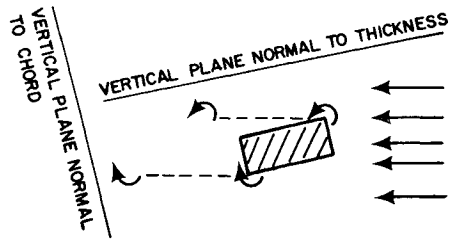

Fig. 6 Vortices shed from rectangular slab.

be used at higher Reynolds numbers. Larger scale phenomena, such as shed vortices, may be calculated with accuracy at high Reynolds number with a much coarser mesh and hence less expenditure of computer time.

Figure 4 shows the axial velocity distribution in a two-dimensional jet in a cross-flow normal to the jet axis,[1] and the expected deformation of the jet into a kidney shape is evident. An example of the application to a three-dimensional jet issuing normally from a plane wall into a cross-flow parallel to the wall[1] is given in Fig. 5. The numerical solution showed a recirculation within the jet in the form of counter-rotating vortices and entrainment of the cross-flow into the rear of the jet. The method also showed the low pressure region behind the jet to be expected from experimental results, and the emission of a vortex ring from the jet exit.

Present Results

All runs in the present application were made with a rectangular body four cells in chord, two in thickness, and eight in span at a cell Reynolds number of 1000, corresponding to a chord Reynolds number of 4000.

Effect of Numerical Parameters

As noted previously, some minimum vorticity magnitude is specified below which vorticity calculated for cells bordering the aggregate of vortex cells is added to adjacent vortex cells rather than a new vortex cell being created. The appropriate stated nondimensional value of 0.01 for this minimum used in previous applications was confirmed in the present application. An increase in this parameter to 0.1 caused an instability peculiar to this numerical procedure that becomes more severe as the time step is decreased. If the minimum vorticity is too large, new vortex cells are not created often enough at small time steps, with the result that the convection and diffusion of vorticity outward is, in effect, reflected back inward at the edge of the aggregate of vortex cells. This effect becomes more pronounced as the time step is decreased, since the probability of a new vortex cell being created decreases with the time step. This instability was not present with a minimum vorticity of 0.01.

Following the indications of all the abovementioned applications, the value of the range beyond which vorticity is

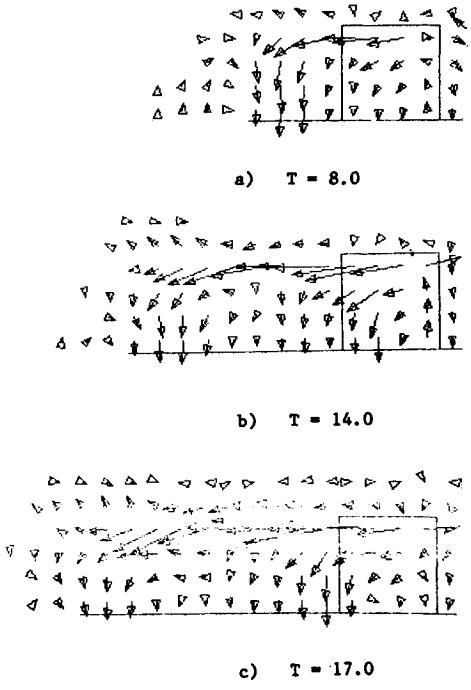

Fig. 7 Vorticity vectors—plane normal to thickness, 1 thickness above body.

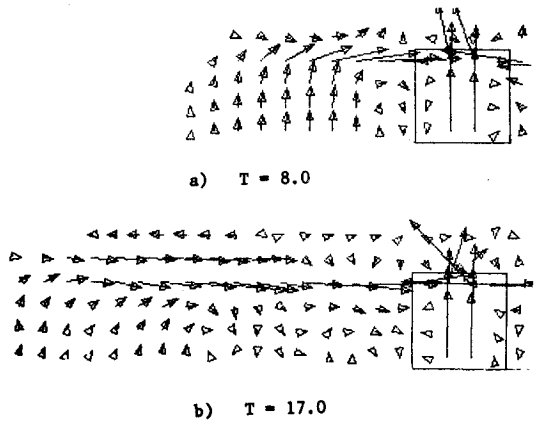

Fig. 8 Vorticity vectors—plane normal to thickness, $\frac{1}{2}$ thickness below body.

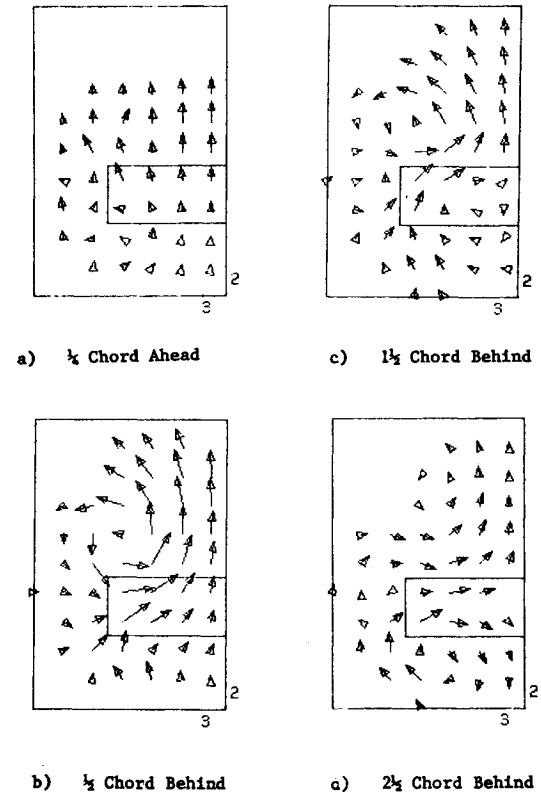

Fig. 9. Velocity vectors—plane normal to chord – T = 17.0.

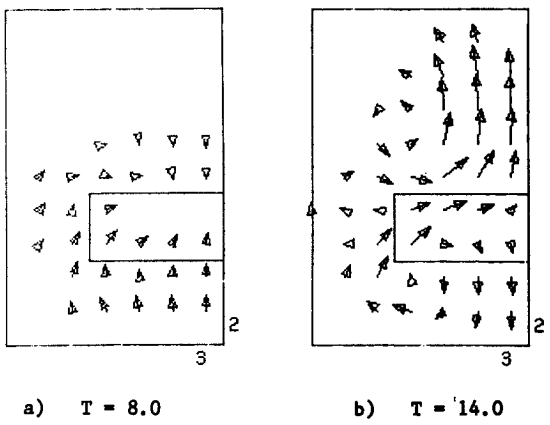

Fig. 10 Velocity vectors—plane normal to chord, $1\frac{1}{2}$ chord behind body.

neglected in the calculation of the velocity was taken as twice the full span of the body. An increase in this parameter by an order-of-magnitude produced only negligible differences.

The effects of an increase in the time step from 0.05 to 0.1 were generally confined at time 9.0 to the second decimal place, though a few differences in the first decimal place occurred in vorticity values. Both time steps were stable, and the larger step was considered adequate for the present application.

Vorticity and Velocity Vectors

The flow pattern for the rectangular body at an angle of attack is a bit more complicated than that of an airfoil and thus requires some explanation. With reference to Fig. 6,¶ the lower left corner of the slab acts as the trailing edge of a body at a small positive angle of attack, while the upper right corner acts as the trailing edge of a body at a large negative angle of attack. It is then to be expected that vortices will be shed at each of these "trailing edges," the vortex shed from the top of the body being the stronger and of sense opposite to that of the usual tip vortex, shed from the bottom of the body in this case.

This behavior is evident in the vorticity and velocity vectors shown in Figs. 7–12.¶ In each of these figures the vectors for the vortex cells in a certain plane are shown projected in that plane. (No cells in front of the body are shown in these figures.) The strong vortex shed from the top of the body is indicated in Fig. 7, which shows vorticity vectors in a plane just above the body. This vortex is carried downstream, trailing a connecting vortex to the tip, and in time a second vortex of the same sense is shed from the top. Figure 8, giving vorticity vectors in a plane just beneath the body, shows the weaker vortex of the opposite sense shed from the bottom of the body, it too being swept downstream trailing a connecting vortex to the tip. These shed vortices are also shown in Fig. 12, in which velocity vectors in planes parallel to the freestream and normal to the span are drawn relative to the freestream velocity.

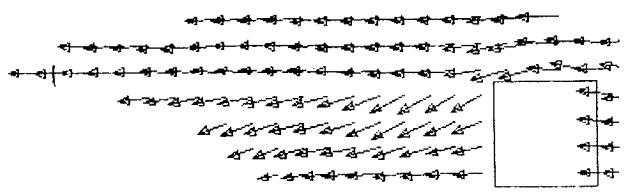

Fig. 11 Velocity vectors—plane normal to thickness, top of body – $T = 17.0$.

¶ The planes cited in Figs. 7–11 are indicated in Fig. 6. The plane of the page in Fig. 8 is the plane cited in Fig. 12.

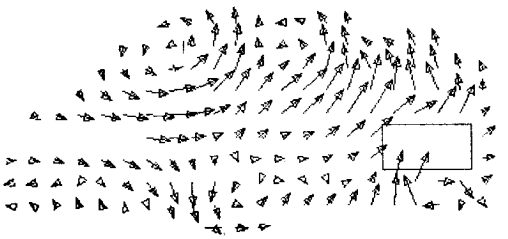

Fig. 12 Velocity vectors relative to freestream—plane normal to span.

There are thus two tip vortices of opposite rotation trailing downstream from the tip, the lower tip vortex having the sense of rotation appropriate to a conventional airfoil. These two tip vortices are evident in the velocity vectors in planes behind the body given in Fig. 9. After the second vortex is shed from the top, the weaker opposite tip vortex from the bottom is overwhelmed near the body but is still evident farther downstream. This process is clearly demonstrated in the time development of these velocity vectors shown by comparison of Figs. 10 and 9c.

Finally, Fig. 11 shows the velocity vectors in a plane through the body parallel to the freestream and parallel to the span. It should be noted in this and all other figures that the vectors nearest the body are not velocities on the body surface, but a half-cell off the surface. The finite extent of these vectors gives the illusion of surface penetration.

Drag Coefficient

The time history of the drag coefficient is shown in Fig. 13. The approach to a steady state is evident. As previously discussed, the accuracy of drag prediction deteriorates as the Reynolds number increases at a fixed cell size, so that, since the cell Reynolds number was of order 10^3 in the present study, this figure is more representative of the development of the drag than it is of its magnitude. In the present application the details of the tip vortex formulation and development were the principal interest.

Conclusions

The versatility of the numerical solution with the integro-differential form of the incompressible Navier-Stokes equations has been further illustrated by the present application showing the formation and development of trailing tip vortices behind a finite rectangular slab at an angle of attack. The intricate flow details described by the present numerical technique for both the present application and the previously-considered jet-in-cross-wind show that the technique can be quite effective in prediction of complicated flow developments and interactions.

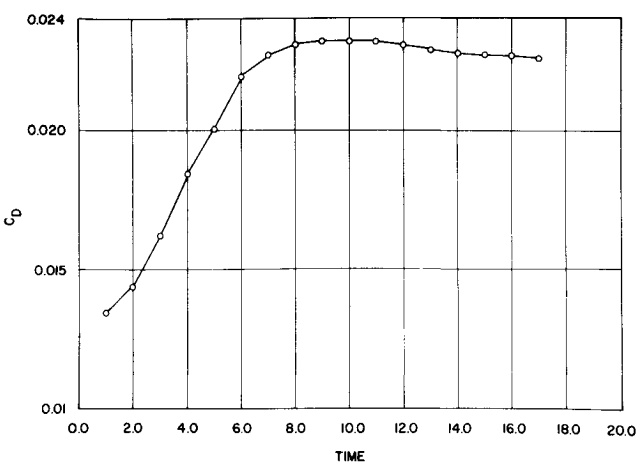

Fig. 13 Drag coefficient development.

Although the requirements for computer time and disk storage are still large, they are orders of magnitude less than what would be required by numerical solution with the differential formulation, so that some time-dependent, three-dimensional solutions can at least be considered within the present state of computer development. The accurate prediction of body forces at high Reynolds numbers would require unfeasible amounts of computer time and storage with a rectangular constant-mesh coordinate system and is still beyond the present development of the technique. Further work would be desirable to extend the present technique to nonrectangular, and eventually general, nonuniform curvilinear coordinate systems, so that bodies of general shape can be more efficiently treated.

References

[1] Thompson, J. F., "Two Approaches to the Three-Dimensional Jet-in-Cross-Wind Problem: A Vortex Lattice Model and a Numerical Solution of the Navier-Stokes Equations," Ph.D. thesis, 1971, Georgia Institute of Technology, Atlanta, Ga.

[2] Wu, J. C. and Thompson, J. F., "Numerical Solution of the Unsteady, Three-Dimensional Navier-Stokes Equations," *Proceedings of Project SQUID Workshop of Fluid Dynamics of Unsteady, Three-Dimensional, and Separated Flows,* Purdue University, Lafayette, Ind., 1971.

[3] Wu, J. C. and Thompson, J. F., "Numerical Solutions of Time-Dependent Incompressible Navier-Stokes Equations Using an Integro-Differential Formulation," *Computers and Fluids,* Vol. 1, 1973, pp. 197–217.

[4] Payne, R. B., "Calculations of Unsteady Viscous Flow Past a Circular Cylinder," *Journal of Fluid Mechanics,* Vol. 4, 1958, pp. 81–86.

[5] Payne, R. B., "A Numerical Method for Calculating the Starting and Perturbation of a Two-Dimensional Jet at Low Reynolds Number," R & M 3047, 1958, Great Britain Aeronautical Research Council, London, England.

[6] Ingham, D. B., "Note on the Numerical Solution for Unsteady Viscous Flow Past a Circular Cylinder," *Journal of Fluid Mechanics,* Vol. 31, 1968, pp. 815–818.

[7] Chorin, A. J., "Numerical Study of Slightly Viscous Flow," *Journal of Fluid Mechanics,* Vol. 57, 1973, pp. 785–796.

[8] Roache, P. J., *Computational Fluid Dynamics,* Hermosa Publishers, Albuquerque, N.Mex., 1972, pp. 9–10.

[9] Karamcheti, K., *Principles of Ideal-Fluid Aerodynamics,* Wiley, New York, 1966, pp. 269–273.

[10] Richtmyer, P. D. and Morton, K. W., *Difference Methods for Initial-Value Problems,* 2nd ed., Interscience, New York, 1967, p. 176.

[11] Shanks, S. P., "An Explicit Numerical Solution of the Three-Dimensional, Incompressible, Time-Dependent Navier-Stokes Equations for a Body with Rectangular Boundaries," M.S. thesis, 1972, Mississippi State University, State University, Miss.

[12] Varga, R. S., *Matrix Iterative Analysis,* Prentice-Hall, Englewood Cliffs, N.J., 1962, pp. 56–59.

JUNE 1974 AIAA JOURNAL VOL. 12, NO. 6

Supersonic, Turbulent Boundary-Layer Separation

C. Herbert Law*
Aerospace Research Laboratories, Wright-Patterson Air Force Base, Ohio

Results are presented of an experimental investigation of turbulent boundary-layer separation in a compression corner in supersonic flow. The experiments were conducted at a freestream Mach number of 2.96 for freestream length Reynolds numbers of 10^7 to 10^8 at adiabatic wall conditions. Surface static pressure measurements, oil flow studies and schlieren and interferometry photographs of the flowfield were made for a series of compression ramp angles so that attached, incipient and well separated turbulent interaction regions could be studied at each freestream condition. The model consisted of a long flat plate followed by an adjustable compression ramp. The turbulent boundary-layer thickness at the compression corner varied between approximately 0.18 in. and 0.12 in. giving a corresponding range of Re_δ of 10^5 to 10^6 for the investigation. The length of the separated region was found to decrease with increasing Reynolds number for fixed compression ramp angle, even when nondimensionalized by the boundary-layer thickness. The incipient separation angle was found to increase with increasing Reynolds number. This result agrees with data obtained by Roshko and Thomke on a wind-tunnel sidewall at higher values of Re_δ.

Nomenclature

C_{f_o} = skin-friction coefficient at beginning of interaction
M = Mach number
p = pressure
$Re_{\infty L}$ = freestream Reynolds number based on flat plate length
Re_δ = Reynolds number based on boundary-layer thickness
T_w = wall temperature
x = axial distance measured along surface from leading edge
α_R = compression ramp angle
δ = boundary-layer thickness

Subscripts
B = beginning of interaction
i = incipient condition
s = condition at the separation point
R = condition at the reattachment point
∞ = freestream condition

Presented as Paper 73-665 at the AIAA 6th Fluid and Plasma Dynamics Conference, Palm Springs, Calif., July 16–18, 1973; submitted July 25, 1973; revision received January 11, 1974.

Index categories: Boundary Layers and Convective Heat Transfer—Turbulent; Supersonic and Hypersonic Flow.

* Research Engineer, Hypersonic Research Laboratory. Member AIAA.

Introduction

MUCH of our knowledge of high-speed turbulent boundary-layer separation is limited to relatively low Reynolds numbers (10^6 to 10^7). The Reynolds numbers associated with